Dyes and Pigments 89 (2011) 137–143

Contents lists available at ScienceDirect

Dyes and Pigments

journal homepage: www.elsevier.com/locate/dyepig

Stability and structural aspects of diketopyrrolopyrrole pigment and its *N*-alkyl derivatives

Jan David [a], Martin Weiter [a], Martin Vala [a], Jan Vyňuchal [b], Jiří Kučerík [a,*]

[a] Faculty of Chemistry, Brno University of Technology, Purkyňova 118, CZ-612 00 Brno, Czech Republic
[b] Research Institute of Organic Syntheses, VUOS, Rybitví 296, CZ-533 54 Rybitví, Czech Republic

ARTICLE INFO

Article history:
Received 29 September 2009
Received in revised form
29 September 2010
Accepted 3 October 2010
Available online 12 October 2010

Keywords:
Diphenyl-diketo-pyrrolo-pyrroles (DPPs)
Pigments
Organic electronics
Thermal stability
Thermogravimetry
Calorimetry

ABSTRACT

An unsubstituted sample, three symmetrically *N*-substituted samples (methyl, butyl and heptyl) and two asymmetrically *N*-substituted samples (butyl and heptyl) of 3,6-diphenyl-2,5-dihydro-pyrrolo[3,4-c] pyrrole-1,4-dione (DPP) were investigated using thermogravimetry and differential scanning calorimetry to reveal the influence on physical-chemical properties of different alkyl chains and symmetry of N-substitution. Stability tests revealed that in all cases the substitution brought significant destabilization of the structure in comparison with the unsubstituted DPP molecule. It was demonstrated that the length of the substituting alkyl chain is a crucial factor in the stability of *N*-alkyl derivatives; the shorter the alkyl chain was, the less stable was the derivative. Further, the symmetrical derivates were less stable than the asymmetrical ones. Unlike the unsubstituted DPP molecule, all the derivatives showed remarkable sensitivity to different cooling regimes which lead to the revealing of monotropical polymorphism in the symmetrical butyl and heptyl derivatives crystalline structure.

© 2010 Elsevier Ltd. All rights reserved.

1. Introduction

Nowadays, a strong effort can be seen in seeking for high-performance and simultaneously photo- and oxidative-thermally stable materials used in organic electronics. Printing technology seems to be a leading technique for cheap large scale production of such devices. Using this technique, the layers of electronic devices are printed employing solutions containing the active materials. However, the increase in solubility can reversibly act on the stability of the materials. Derivatives of 3,6-diphenyl-2,5-dihydro-pyrrolo[3,4-c]pyrrole-1,4-dione, commonly referred as DPPs, are potentially attractive materials for organic electronics. They belong to important industrial high-performance pigments [1] showing significantly high melting points with respect to other low molecular pigment standards. They also exhibit remarkable resistance against chemical, heat, light and climate influences. There is a wide range of possible applications which have been already investigated covering e.g. latent pigments [2], solid state dye lasers [3], gas detectors [4,5] or electroluminescent devices [6,7].

The DPPs are usually insoluble in common solvents [8]. One of the reason for their low solubility is the existence of hydrogen bondings between the H atom of the nitrogen functional group and oxygen. The unsubstituted DPP is perfectly planar, the $\pi-\pi$ electrons stacking occurs in solid state and also contributes to their insolubility. In order to modify the solubility, it is necessary to carry out either the N-substitution and/or the breaking of the molecule planarity [8]. In our previous work [7], we discussed the influence of N-alkylation on optical properties, and the results were correlated with molecule geometry calculated by quantum chemical methods. It was found that while the parent DPP molecule (abbreviated as DPP in this work) is perfectly planar, the N-substitution causes rotation of the adjacent phenyl rings (see Fig. 1) and thus reducing the effective conjugation extent. This, in turn, causes hypsochromic shift of the absorption spectrum. Simultaneously, the fluorescence spectra move to the longer wavelength region increasing Stokes shifts. The effect is more pronounced for the double *N*-alkylated derivatives. Since the angle of distortion is not dependent on the length of the substituent, no differences between butyl substituted (DPP-B, DPP-BB) and heptyl substituted derivatives (DPP-H, DPP-HH) were found [7].

The stability and behavior of physical structure of photo-sensitive materials which were exposed to different thermal history is very important. In order to produce high quality devices in a controlled way, knowledge about the crystallinity, and polymorphism seems to be crucial. Since physical properties of polymorphs can significantly differ, polymorphism can cause

* Corresponding author. Tel.: +420 5 41 14 94 85; fax: +420 5 41 21 16 97.
E-mail address: kucerik@fch.vutbr.cz (J. Kučerík).
URL: http://www.fch.vutbr.cz/home/kucerik

0143-7208/$ – see front matter © 2010 Elsevier Ltd. All rights reserved.
doi:10.1016/j.dyepig.2010.10.001

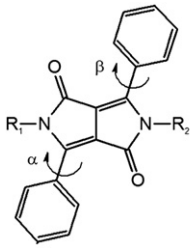

	R_1	R_2
DPP	H	H
DPP-MM	CH_3	CH_3
DPP-B	C_4H_9	H
DPP-BB	C_4H_9	C_4H_9
DPP-H	C_7H_{15}	H
DPP-HH	C_7H_{15}	C_7H_{15}

Fig. 1. The basic structure of 3,6-diphenyl-2,5-dihydro-pyrrolo[3,4-c]pyrrole-1,4-dione (DPP), also known as DPP and the respective derivatives used in this study. The definition of calculated torsion angles α and β can be found in [7].

troubles in technological applications [15]. Essentially, the difference in crystal structure leads to different optical properties, structural stability, solubility, melting temperature, enthalpy etc. Since the crystallization of one specific polymorph is controlled by a combination of thermodynamic and kinetic factors [9], it is important to determine the relationship between such fraction and the others in the polymorphs mixture.

In this study, using thermogravimetrical analysis (TGA), our research was extended by the thermal and thermo-oxidative stability tests and by distinguishing between processes of evaporation or degradation. In fact, materials DPP and DPP-MM have already been investigated by TGA [10]; however, the large set of DPP materials and comparison of their properties can bring deeper insight into the physical chemistry of such interesting pigments. Furthermore, employing differential scanning calorimetry (DSC) we would like to shed light on the structural variability of investigated samples after different thermal history. The obtained results are discussed with respect to the chemical structure of the studied molecules.

2. Experimental

2.1. Materials

Samples of the studied derivatives were synthesized in VUOS, a.s. (Research Institute of Organic Syntheses, Inc., Rybitvi, Czech Republic) according to the procedures described in [7,8]. One unsubstituted sample (DPP), three symmetrically *N*-substituted samples (DPP-MM – methyl group substituted, DPP-BB – butyl group substituted and DPP-HH – heptyl group substituted) and two asymmetrically substituted samples (DPP-B with butyl group and DPP-H with heptyl group) were investigated in this study. Molecular structures of investigated samples are depicted in the Fig. 1.

Before all the experiments had been performed, the compounds were carefully milled in the agate mortar in order to maintain uniform heat flow to the whole dosing of sample in both thermal analysis methods.

2.2. Methods

2.2.1. Thermogravimetric analysis

Thermogravimetric studies were performed using TA Instruments TGA Q5000 (New Castle, DE, U.S.A.) device in 100 μL open platinum pans. The samples, typically 5 mg, were heated by using thermal ramp of 10 °C min^{-1} from 40 °C to 650 °C in either dynamic atmosphere of nitrogen (thermal stability) or air (thermo-oxidative stability). Flow rate of both gases was 25 mL min^{-1}.

2.2.2. Differential scanning calorimetry

Calorimetric analyses were carried out employing TA Instruments DSC Q200 equipped with an external cooler RCS90 allowing experimental temperature range from −90 to 400 °C. Experiments were conducted in open TA Tzero™ aluminum pans. The first heating run was conducted at 10 °C min^{-1} from 40 °C to the temperature 5 °C lower than the degradation temperature onset (T_{onset}) previously determined by using thermogravimetry under nitrogen. In order to simulate the moderate temperature decrease, cooling ramp of 0.5 °C min^{-1} was applied to reach −90 °C, followed by 1 min of isothermal stage. The first calorimetric measurement was performed using heating ramp of 10 °C min^{-1} from −90 °C to the temperature (T_{onset} − 5)°C. The second experiment was performed using the same heating ramp after the rapid equilibration of the sample down to −90 °C and 1 min of isothermal stage. It is necessary to point out that in this case, the averaged temperature of cooling exceeded 20 °C min^{-1}. All DSC experiments were made under 50 mL min^{-1} of nitrogen purge. The device was calibrated for temperature and enthalpy using indium, tin and zinc standards (Perkin Elmer). Additional measurement of sample DPP was carried out also by the TA Instruments Q600 (simultaneous DSC and TGA) under the same conditions as described above. All the records were assessed by TA Universal Analysis 2000 software version 4.4A.

3. Results

3.1. Stability tests – thermogravimetric analysis (TGA)

TGA measurements were conducted to test the temperatures of mass loss occurrence. These temperatures correspond either to the temperature of degradation (T_D), evaporation (T_{ev}) or sublimation (T_s). The character of two latter phenomenons was revealed by DSC. In principle, if the sample shows an endotherm on DSC record, the sample is melted and therefore, the temperature can be associated to evaporation. On the contrary, if DSC record does not show any melting, the sample is solid and the process can be attributed to the sublimation.

In order to distinguish between T_s and T_{ev} or T_s, the mass loss and its first (DTG) and second temperature derivative curves were used. The clarification of such an approach is explained further in the text. The typical TGA record and its DTG curve were obtained by using conditions described in Experimental part for sample DPP-MM and is reported in Fig. 2. In this work, the DTG is plotted in an inverse mode to improve the illustrative quality of Figures. Since the TGA record provides an integral piece of information regarding the mass loss, DTG or potential second derivation allows a closer look into the dynamics of the processes and frequently helps to distinguish the change in mass loss mechanism.

Sample DPP showed no event on the DSC curve when we used the temperature program reported in Experimental section. Therefore, in order to discover potential melting at temperatures above sublimation, the simultaneous DSC and TGA was carried out (Fig. 3). As it can be seen on the DSC curve, no overlapping of enthalpy processes occurred, and thus the sample cannot be melted under conditions used in this work. The respective 1st and 2nd derivative curves of TGA of DPP are reported in Fig. 4.

The results obtained from DTG records are summarized in Table 1. All of the samples in both atmospheres showed one or two degradation steps. If occurred, the second degradation step was only minor and was not taken for further assessment. The onset of a process in DTG is traditionally determined from the 1st derivative mass loss curve. However, it is clear that the determined temperature does not indicate whether the temperature corresponds to the degradation or to the evaporation. The determined onset only indicates the beginning of mass changes which can be attributed to both above-mentioned processes. Therefore, the 2nd derivative was carried out in order to enable the separation of possible overlapping processes. An example of such a separation for sample DPP is

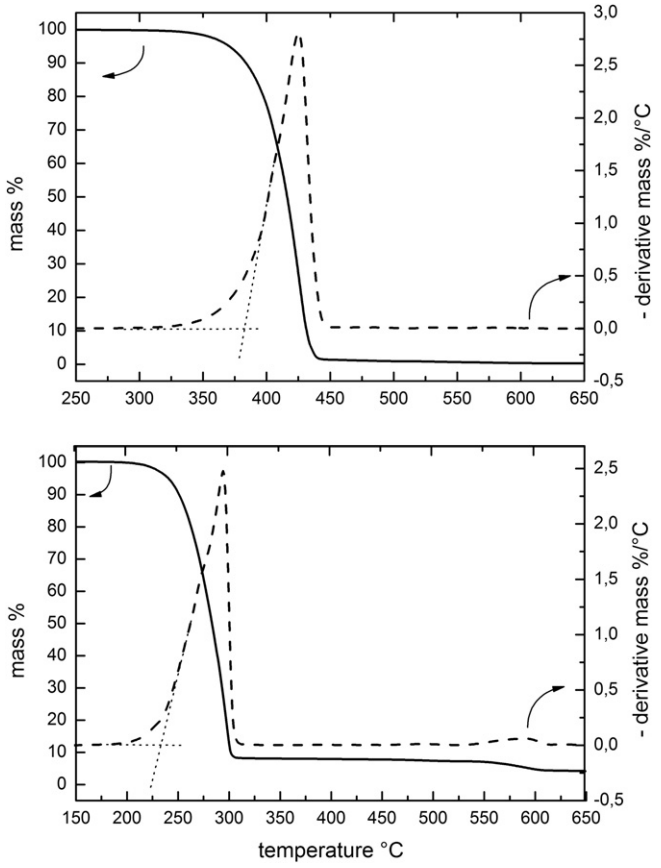

Fig. 2. TGA heating run for the DPP-alkyl derivate DPP-MM in the atmosphere of nitrogen. Onset temperatures are summarized in Table 1.

reported in Fig. 4. Therefore, Table 1 reports the two temperatures, i.e. T_{ev} (mass loss without degradation) and T_D (mass loss connected with degradation). The only exception is the sample DPP, which showed no melting, and therefore, had no T_{ev} but a temperature of sublimation T_s. All T_{ev} and T_s occurred in the temperature range from 238 °C to 383 °C. As it can be seen in Table 1, thermal-oxidative stability results (experiments in air) are similar to the thermal stability results (experiments in N_2), but generally shows a slight shift to lower temperatures. As expected, the thermal stability of investigated materials is slightly higher than the thermal-oxidative

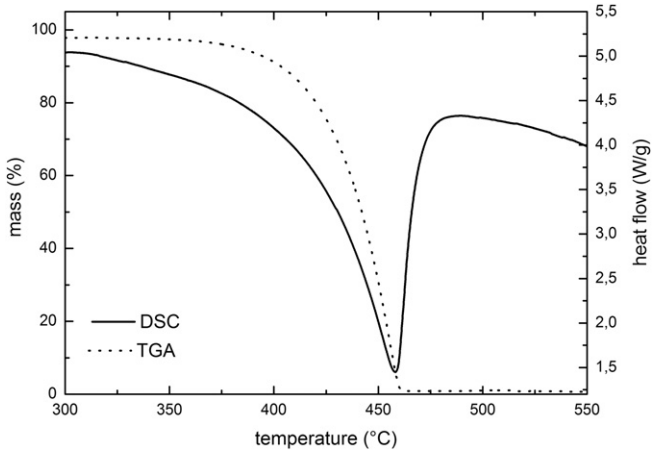

Fig. 3. Simultaneous DSC and TGA record of sample parental sample DPP.

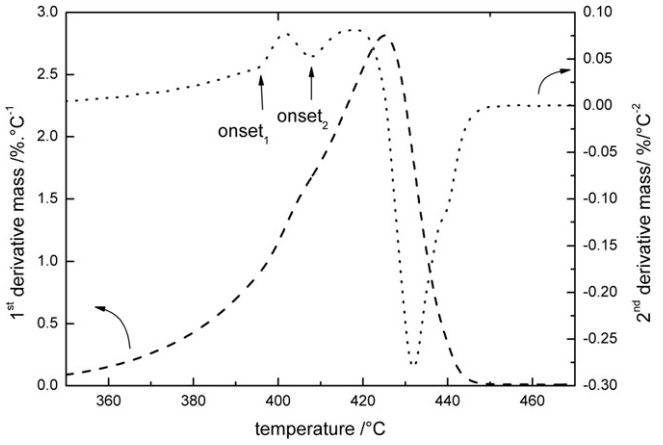

Fig. 4. Determination of the onset$_1$ and the onset$_2$, i.e., distinguishing between sublimation and degradation of sample DPP. Other samples exhibited melting and therefore, the onset$_1$ stands for evaporation temperature in this case.

stability. Comparison of T_D showed the thermal stability of samples in order of DPP > DPP-HH > DPP-B > DPP-MM > DPP-BB; sample DPP-H could not be taken into account since the whole sample was completely evaporated at 350 °C. In dynamic air atmosphere, the thermo-oxidative stability showed following order of DPP > DPP-HH > DPP-B = DPP-H > DPP-MM > DPP-BB. DPP-H sample was included in this order since the thermo-oxidative stability showed lower temperature than the T_{ev}, which suggests that the degradation under air occurs earlier than the evaporation. As stated in the Experimental part, the temperatures of T_{ev} and onsets$_1$ (see Fig. 4) were used to design the DSC experiments (to suggest upper temperature limit). The T_s and T_{ev}, indicating the temperature at which the molecular vibrations overcame the weak intermolecular interactions stabilizing structures either in solid state (DPP4) or in melted (the rest), are ordered as follows: DPP4 > DPP-H > DPP-HH > DPP-B > DPP-BB > DPP-MM.

3.2. Phase transitions – differential scanning calorimetry (DSC)

DSC experiments revealed additional differences in physical structure of investigated materials. Most of the derivatives, when heated from −90 °C expressed several phase transitions which varied depending on the chemical structure and thermal history of the respective samples. DSC records of selected samples are given in Figs. 5 and 6, for samples DPP-BB and DPP-HH, respectively. Table 2 summarizes main phase transitions such as melting, crystallization and glass transition of measured samples. Minor transitions, which

Table 1
Thermogravimetric analyses results. The onset$_1$ suggests the temperature of evaporation, the onset$_2$ indicates possible beginning of degradation.

Sample	Purge gas	Onset$_1$ [°C]	Onset$_2$ [°C]	Char [%wt]	Steps
DPP	N_2	383	396	0.4	1
DPP	air		356	0	1
DPP-MM	N_2	238	262	3.8	2
DPP-MM	air		237	0	2
DPP-B	N_2	269	281	0.1	1
DPP-B	air		267	0	2
DPP-BB	N_2	241	246	0	1
DPP-BB	air		234	0	2
DPP-H	N_2	290	E	0	1
DPP-H	air		267	0	2
DPP-HH	N_2	282	290	0	1
DPP-HH	air		271	0	1

E – sample was completely evaporated, no degradation was observed.

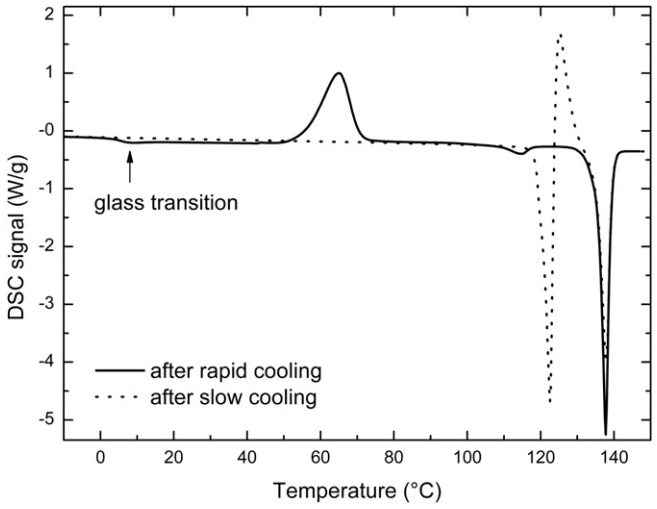

Fig. 5. Comparison of DSC records for sample DPP-BB after different cooling regime. Moderate cooling regime was 0.5 °C per min from 200 to −90 °C, heating 10 °C per min.

are not important for further discussion, are only described in the next paragraphs.

DSC record of DPP sample after both moderate and rapid cooling did not show any event at lower temperatures (Fig. 3). In contrast, at elevated temperatures the simultaneous DSC/TGA record showed an intensive endothermal peak with no shoulder accompanied by a massive mass loss which can be attributed to the sublimation of the sample followed by degradation (cf. Table 1).

After moderate and rapid cooling DSC record of DPP-MM sample showed endothermal melting peaks around 234 °C with melting enthalpy around 112 J g^{-1}, which indicates no influence on the sample thermal history.

Moderate cooling ramp caused a tiny exotherm probably corresponding to the cold crystallization of DPP-B with onset at −19 °C (enthalpy 0.43 J g^{-1}) and followed by an endotherm corresponding to the melting at −8 °C (peak temperature −5 °C, melting enthalpy 0.26 J g^{-1}). Further, at 10.7 °C an endotherm appeared again indicating the structure melting (peak temperature 17 °C, melting enthalpy 0.18 J g^{-1}). A glass transition with midpoint at −18 °C was observed in the record after rapid cooling ramp.

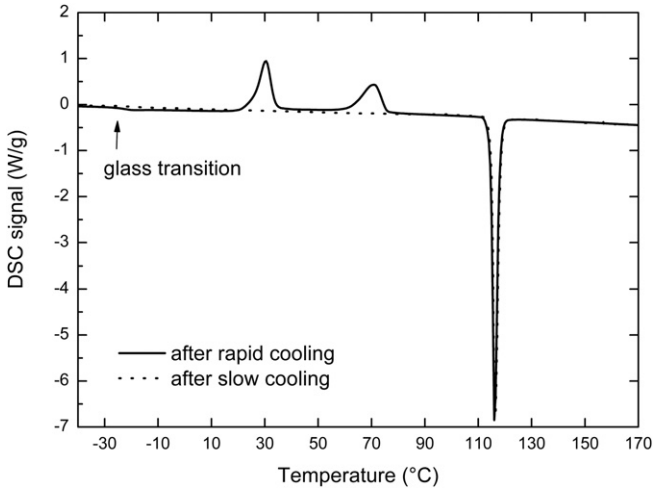

Fig. 6. Comparison of DSC records for sample DPP-HH after different cooling regime. Moderate cooling regime was 0.5 °C per min from 200 to −90 °C, heating 10 °C per min.

One of the most complex calorimetric results was given by the measurement of the sample DPP-BB. DSC records after the moderate cooling ramp resulted in three consecutive and intensive phase transitions; melting at 120 °C (melting enthalpy 72.3 J g^{-1}), followed by cold crystallization at 124 °C (peak temperature 125 °C, enthalpy of crystallization 38.5 J g^{-1}) and subsequent second melting peak at 135.2 °C (melting enthalpy 70.9 J g^{-1}). Calorimetric results from the experiment after the rapid cooling ramp showed a glass transition with midpoint of 5 °C, a cold crystallization at 56 °C (enthalpy of crystallization 69 J g^{-1}). After that, a slight melting peak at 108 °C was detected (melting enthalpy 6.1 J g^{-1}) followed by intensive melting at 136 °C (melting enthalpy 84 J g^{-1}), which was observed in the experiment after moderate cooling rate as well.

Heating run after moderate cooling of sample DPP-H resulted in a cold crystallization at −41 °C with peak temperature of −26 °C and crystallization enthalpy of 1.85 J g^{-1} followed by melting at 0 °C and peak temperature at 2 °C and melting enthalpy of 1.09 J g^{-1}. After rapid cooling, the DPP-H sample showed two consequent melting peaks at −19 °C (peak temperature at −16 °C, melting enthalpy of 0.04 J g^{-1}) and at −12 °C (melting enthalpy of 0.24 J g^{-1}), respectively. Both temperature regimes performed similar melting peaks around 212 °C (enthalpies around 100 J g^{-1}).

Complicated results were obtained from calorimetric experiments in the sample DPP-HH as well. After moderate cooling, significant melting at 115 °C with peak temperature of 116 °C and melting enthalpy of 96.3 J g^{-1} was detected. After a rapid cooling, a glass transition with midpoint at −22 °C was observed followed by two cold crystallization peaks. The first crystallization peak occurred at 25 °C, with temperature of the peak at 31 °C and crystallization enthalpy of 37.4 J g^{-1}. The second cold crystallization event was less prominent and appeared at 62 °C with peak temperature of 71 °C and crystallization enthalpy of 30.7 J g^{-1}. The same melting peak, as observed in the experiment after moderate cooling, was detected also after rapid cooling, i.e., the onset at 115 °C, peak temperature at 116 °C and melting enthalpy of 95.4 J g^{-1}.

In contrast to the order of T_{ev}, the temperatures of crystal melting followed reverse order, i.e., DPP-MM > DPP-BB > DPP-HH > (DPP). Similar order can be seen for asymmetrical samples onsets DPP-B < DPP-H and for melting temperatures of DPP-B > DPP-H.

4. Discussion

Table 1 indicates significant distinctions in stability and structural feature of investigated samples. First of all, there has been observed a great difference between substituted derivates and unsubstituted DPP. In fact, all the substituted samples were less stable thermally (except DPP-H where stability could not be determined) than the unsubstituted parent sample DPP. The onset temperature of degradation 238 °C found for the least stable derivative DPP-MM is about 145 °C lower compared to the DPP (383 °C). Table 1 summarizes the data obtained from TGA under inert atmosphere and oxidative atmosphere of air. As can be seen in several cases, the temperatures of evaporation in nitrogen are similar to those obtained in air (i.e., DPP-MM, DPP-B and possibly DPP-BB). That suggests that in those samples, oxygen did not play an important role in their degradation.

The highest stability of DPP can be easily explained with respect to its structure. As already mentioned, overlapping of π−π electrons between adjacent molecules occurs due to the planarity of the molecule [8]. The compact and rigid structure is stabilized by four intermolecular hydrogen bonds per molecule between the −NH group of one molecule and the oxygen atom of the neighboring one

Table 2
Comparison of results obtained by DSC measurement for samples which underwent different thermal history. For better understanding only major events are given, the rest can be found in the text. DPP is not reported due to the absence of significant transitions.

Thermal history	Sample	Crystallization I		Crystallization II		Melting I		Meting II		Glass transition
		T_{onset} [°C]	ΔH [J g^{-1}]	T_{onset} [°C]	ΔH [J g^{-1}]	T_{onset} [°C]	ΔH [J g^{-1}]	T_{onset} [°C]	ΔH [J g^{-1}]	$T_{midpoint}$ [°C]
moderate cooling	DPP-MM	–	–	–	–	234.4	109.4	–	–	–
rapid cooling	DPP-MM	n.d.	n.d.	n.d.	n.d.	n.d.	n.d.	n.d.	n.d.	n.d.
moderate cooling	DPP-B	–	–	–	–	245.4	93.8	–	–	–
rapid cooling	DPP-B	–	–	–	–	244.6	92.5	–	–	−18.3
moderate cooling	DPP-BB	123.9	38.5	–	–	120.1	72.3	135.2	70.9	–
rapid cooling	DPP-BB	55.5	69.0	–	–	108.3	6.1	135.6	83.9	5.1
moderate cooling	DPP-H	–	–	–	–	211.9	75.8	–	–	–
rapid cooling	DPP-H	–	–	–	–	212.1	74.9	–	–	–
moderate cooling	DPP-HH	–	–	–	–	115.2	96.3	–	–	–
rapid cooling	DPP-HH	25.3	37.4	62.1	30.7	114.7	95.4	–	–	−22.2

along the *b* axis [11]. This interaction further contributes to the insolubility of the non-*N*-substituted DPPs. In DPP, the number of atomic contact along the stacking axis is 9 [12]. That number strongly depends on the character of the N-substitution of the derivate [13]. Therefore, the existence of hydrogen bonds between the −NH group and oxygen on the central pyrrolo-pyrrole core additionally increases the energy needed for molecule defragmentation as confirmed by T_{ev} or T_s or degradation T_D. On the contrary, it has been stated that the torsion angles between the central pyrrolo-pyrrole part and the phenyls are independent of the alkyl length [7], therefore, the difference between derivates with different alkyl length has to be related to different properties.

Remaining char observed on TGA for DPP sample confirms the hypothesis about the degradation which follows the sublimation or evaporation. Traditionally, the DPP pigments are deposited on a surface at elevated temperatures. The char formation indicates that choosing an inappropriate temperature can lead to the pigment degradation since T_s and T_D of this sample are not significantly different. In TGA experiments the linear heating is employed which implies that the sample has not enough time to sublimate completely from the pan. In technological (industrial) practise this problem can be (and usually is) solved by pressure reduction [12]. It is clear that the processes of evaporation are relatively moderate and since the temperature of degradation is shifted only 15 °C higher, the deposition under vacuum is necessary.

The introduction of two methyl groups to the nitrogen atoms breaks the planarity of the molecule [7] decreasing the strength of H-bonds and consequently causes easier defragmentation of the molecule. That can be identified in the sample DPP-MM which showed the lowest onset on DTG plot. Since T_{ev} and T_D in air are similar, it could be expect that the temperature is associated with sample's evaporation. However, as suggested by TGA analysis in nitrogen, that temperature is again either close or identical to the temperature of sample degradation since there was a char observed at the end of the analysis at 650 °C. In contrast, it can be seen that N-substitution by methyl groups in sample DPP-MM caused relatively high melting temperatures of present crystals (very close to the temperature of evaporation/degradation) with the highest melting enthalpy in comparison with other samples. Unlike the other samples, DPP-MM was not able to be measured after different thermal history due to the vicinity of both temperatures. The value of melting enthalpy reported in Table 2 can also be biased by processes occurring simultaneously.

A similar situation was observed for sample DPP-B. Unlike the sample DPP-MM, DPP-B presents an asymmetrical derivate of DPP which seems to increase both temperatures of evaporation and crystal melting. Again, the temperatures of degradation determined using TGA in both atmospheres were very close to each other suggesting the same explanation as given for DPP-MM sample, i.e. sample is simultaneously evaporated and decomposed above T_{ev}. That observation is confirmed by the presence of char at 650 °C (Table 1).

An increase in the onset temperature was observed also for the second asymmetrical sample DPP-H. The significant difference in the onset temperatures obtained under different conditions indicates the decrease of thermo-oxidative resistance with the increasing length of alkyl chain. This can be interrelated to the decrease in temperature of crystal melting in the sample. It is our hypothesis that alkyl chains have higher molecular motion after the crystalline structure melting and reactive gas can easily diffuse through the sample. It is well known that aliphatic chains are relatively unstable under a thermo-oxidative attack [14], hence, the stability of the derivatives under study decreases with the increasing length of alkyl chain.

Table 2 reports that asymmetrical molecules, i.e. samples DPP-B and DPP-H did not show any response to the different thermal history which implies a relatively easy molecular transport to form crystals and no tendency to polymorphism. In contrast, symmetrical molecules with longer alkyl chains DPP-BB and DPP-HH seem to have tendency to form different crystalline forms resulting in occurrence of multiple peaks in DSC signal. In contrast to the sample DPP-HH, when the DPP-BB sample was cooled rapidly, the enthalpy of melting dropped down which indicates that the molecular motion during the crystal formation of both samples was disturbed by different extraneous factors. Moderate cooling of sample DPP-BB gave melting-crystallization-melting sequence while DPP-HH simply melted in one step and at lower temperature than DPP-BB. When cooled quickly, DPP-HH pre-crystallized in two steps while the onset of the first melting was at lower temperature than that for sample DPP-BB. That implies that in the first stage the longer alkyl chains in sample DPP-HH needed lower energy input to re-crystallize rather than the shorter chain in sample DPP-BB. Accordingly, inspired by melting temperatures and enthalpies of pure alkanes, it is supposed that there is a hindrance in molecular motion in C_4H_9 alkyl chain reducing the rate of crystallization. There is a possible explanation that the DPP molecular skeleton has an influence on the alkyl chain via van der Waals interactions. In fact, the first carbons of alkyl chain can be affected by the presence of neighboring electron acceptor atom having a great influence on the molecular motion of the whole chain. The other possibility is that the molecular motion is influenced by the whole DPP skeleton and the C_4H_9 chain length is not long enough to overcome the electrostatic interactions between adjacent DPP molecules. Since there is a strong intermolecular interaction between oxygen lone electron pair and hydrogen of −NH group [18], it seems that the H atom can be substituted in its role by short alkyl chain since the

melting of DPP-MM sample is relatively high; on the contrary, the temperature of degradation/evaporation is very close, as a result the H-bonds formed by –NH group is weaker and consequently destabilizes the structure at relatively low temperatures.

Using the nomenclature of Lehman [15], enantiotropic polymorphism pertains two crystal forms that undergo reversible phase exchanges between one another, while monotropic polymorphism corresponds to two crystal forms where one – a kinetically trapped, metastable form – undergoes an irreversible phase change to the other thermodynamically more stable form [16]. Fig. 5 indicates two crystalline structures present in sample DPP-BB represented by two endothermal melting peaks. Clearly, the existence of the less stable form depends on the rate of cooling, so it is kinetically governed and therefore the sample crystalline structure is monotropically polymorphous. In the case of sample DPP-HH (Fig. 6), after cooling the kinetically most favorable polymorph crystallized first and subsequently transformed into thermodynamically stable one. Again, such behavior can be attributed to the monotropic polymorphism.

Fruitful discussion can be held after comparison of mono-substituted and bi-substituted derivatives. The T_Ds obtained for the mono-substituted derivatives were always higher than those for the bi-substituted. A possible explanation implies the electron donating character of the alkyl groups. Due to the mesomeric effect between the nitrogen and oxide atoms, the electron density is unequally distributed over the molecule and creates a dipole. The alkylation even increases the mesomeric effect and consequently increases the polarity of the molecule. This can be experimentally observed as a blurring of vibrational structure of electron spectra [7,16,17]. Therefore, the electron donating character of the substituted alkyls increases reactivity and consequently causes easier defragmentation of the molecule. As a result the mono-substituted derivatives are thermally more stable because of their lower reactivity.

In order to support our statement about the evaporation followed by degradation, the DPP-MM sample was thermally treated at specific temperatures and the sample composition was followed by FTIR analysis (KBr pellet technique). As shown in Fig. 7, at temperature 260 °C, i.e., 3 °C below the predicted decomposition temperature, the sample still resembled the molecular character of DPP-MM. At 280 °C the FTIR spectra showed a shift in intensities at several wave numbers, and the shift continued with increasing temperature (not shown). The attribution of peaks wave numbers to bond vibrations can be found for example in [3]. It was impossible to determine the exact temperature at which the change of structure occurred since the degradation did not take part in the whole volume of the sample. Indeed, the changes were observable at first sight, the color of the pigment changed from red to orange at 280 °C and greenish above 300 °C.

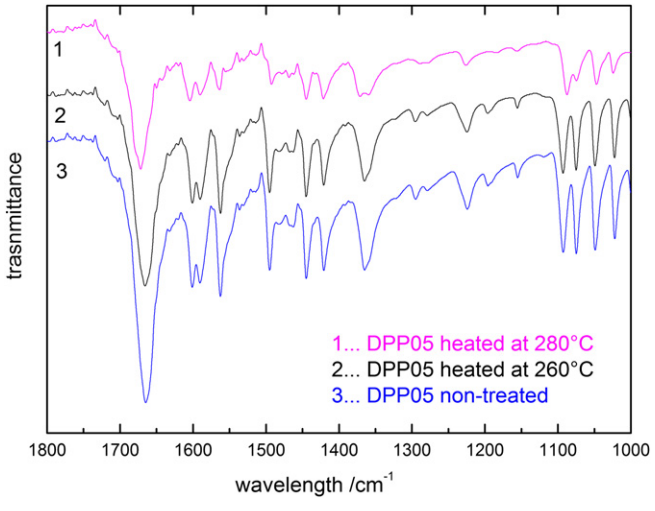

Fig. 7. Comparison of FTIR records of sample DPP-MM, and DPP-MM heated up to 260 and 280 °C. The Figure shows only selected wavenumbers range.

5. Conclusion

One unsubstituted sample, three symmetrically *N*-substituted samples (methyl, butyl and heptyl) and two asymmetrically *N*-substituted samples (butyl and heptyl) of 3,6-diphenyl-2,5-dihydro-pyrrolo[3,4-c]pyrrole-1,4-dione were investigated to observe the influence on physical-chemical properties of different alkyl chains and symmetry of substitution. From the point of view of their evaporation temperature, thermal stability and thermo-oxidative stability, it was revealed that substitution brought about significant destabilization of the structure in comparison with parental molecule. It was demonstrated that the length of the substituting alkyl chain is a crucial factor in their stability; the shorter chain the less stable derivate was obtained while the symmetrical derivates were less stable than asymmetrical ones. As revealed by DSC, unlike the other samples, the symmetrical derivates indicated monotropical polymorphism. On the contrary, DSC experiments did not reveal the presence of different crystalline structures in DPP, although the presence of two crystalline forms was reported [19]. It seems that the thermal agitation (and therefore DSC) is not a suitable manner for transformation of those phases, it is likely that the aforementioned weak interactions are strong enough to resist their vibration upon heating.

Acknowledgements

The financial support of the Ministry of Education of the Czech Republic – project MSM 0021630501 and the Academy of Sciences of the Czech Republic – project KAN401770651 are acknowledged.

References

[1] (a) Rochat AC, Cassar L, Iqbal A. EP 94911; 1983. (b) Iqbal A, Pfenninger J, Rochat AC, Babler F. EP 181290; 1989. (c) Pfenninger J, Iqbal A, Rochat AC, Wallquist O. USP 4778899; 1986. (d) Surber W, Iqbal A, Stern C. EP 302018; 1989. (e) Wooden G, Schloeder I, Wallquist O. EP 672729; 1995. (f) Hendi SB. EP 962499; 1999.
[2] Zambounis JS, Hao Z, Iqbal A. Latent pigments activated by heat. Nature (London) 1997;388(6638):131–2.
[3] Fukuda M, Kodama K, Yamamoto H, Mito K. Evaluation of new organic pigments as laser-active media for a solid-state dye laser. Dyes and Pigments 2004;63(2):115–25.
[4] Mizuguchi J, Imoda T, Takahashi H, Yamakami H. Polymorph of 1,4-diketo-3,6-bis-(4'-dipyridyl)-pyrrolo-[3,4-c]pyrrole and their hydrogen bond network: A material for H2 gas sensor. Dyes and Pigments 2006;68(1):47–52.
[5] Hoki T, Takahashi H, Suzuki S, Mizuguchi J. Hydrogen gas sensor based upon proton acceptors integrated in copper-tetra-2,3-pyridinoporphyradine. IEEE Sensors Journal 2007;7(5):808–13.
[6] Beyerlein T, Tieke B, Forero-Lenger S, Brütting W. Red electroluminescence from a 1,4-diketopyrrolo[3,4-c]pyrrole (DPP)-based conjugated polymer. Synthetic Metals 2002;130(2):115–9.
[7] Vala M, Weiter M, Vyňuchal J, Toman P, Luňák Jr S. Comparative studies of diphenyl-diketo-pyrrolopyrrole derivatives for electroluminescence applications. Journal of Fluorescence 2008;18(6):1181–6.
[8] Potrawa T, Langhals H. Fluorescent dyes with large stokes shifts – soluble dihydropyrrolopyrrolediones. Chemische Berichte 1987;120(7):1075–8.
[9] Aret E, Meekes H, Vlieg E, Deroover G. Polymorphic behavior of a yellow isoxazolone dye. Dyes and Pigments 2007;72:339–44.
[10] Mizuguchi J, Wooden G. A large bathochromic shift from the solution to the solid state in 1,4-diketo-3,6-diphenyl-pyrrolo-[3,4-c]-pyrrole. Berichte der Bunsen-Gesellschaft für Physikalische Chemie 1991;95:1264–74.
[11] Mizuguchi J. Correlation between crystal and electronic structures in diketo-pyrrolopyrrole pigments as viewed from exciton coupling effects. Journal of Physical Chemistry A 2000;104:1817–21.

[12] Mizuguchi J, Grubenmann A, Wooden G, Rihs G. Structures of 3,6-diphenylpyrrolo[3,4-c]pyrrole-1,4-dione and 2,5-dimethyl-3,6-diphenylpyrrolo [3,4-c]pyrrole-1,4-dione. Acta Crystallographica 1992;B48:696–700.
[13] Weiter M, Salyk O, Bednář P, Vala M, Navrátil J, Zmeškal O, Vyňuchal J, Luňák Jr. S. Morphology and properties of thin films of diketopyrrolopyrrole derivatives, Materials Science and Engineering: B, submitted for publication.
[14] Válková D, Kislinger J, Pekař M, Kučerík J. The kinetics of thermo-oxidative humic acids degradation studied by isoconversional methods. Journal of Thermal Analysis and Calorimetry 2007;89:957–64.
[15] Lehman O. Die krystallanalyse. Leipzig: Wilhelm Engelmann; 1891.
[16] Hauser MR, Zharakov L, Doxsee KM, Tonglei L. Polymorphism of a simple organic amide. Crystal Growth and Design 2008;8(12):4428–31.
[17] Luňák S, Vyňuchal J, Vala M, Havel L, Hrdina R. The synthesis, absorption and fluorescence of polar diketo-pyrrolo-pyrroles. Dyes and Pigments 2009;82:102–8.
[18] Vala M, Vyňuchal J, Toman P, Weiter M, Luňák Jr S. Novel soluble diphenyl-diketo-pyrrolopyrroles. Experimental and theoretical study. Dyes and Pigments 2009;89:102–8.
[19] Hao Z, Iqbal A. Some aspects of organic pigments. Chemical Society Reviews 1997;26:203–13.